Transport properties in asymmetric InAs/AlSb/GaSb electron-hole hybridized systems

Kyoichi Suzuki
NTT Basic Research Laboratories, NTT Corporation, 3-1 Morinosato-Wakamiya, Atsugi-shi, Kanagawa, 243-0198 Japan

Sen Miyashita
NTT Advance Technology Corporation, 3-1 Morinosato-Wakamiya, Atsugi-shi, Kanagawa, 243-0198 Japan

Yoshiro Hirayama
NTT Basic Research Laboratories, NTT Corporation, 3-1 Morinosato-Wakamiya, Atsugi-shi, Kanagawa, 243-0198 Japan and CREST-JST, Kawaguchi-shi, Saitama, 331-0012 Japan

(Received 25 July 2002; revised manuscript received 17 January 2003; published 15 May 2003)

Transport properties in asymmetric InAs/GaSb and InAs/AlSb/GaSb heterostructures sandwiched by AlGaSb layers were studied. For the InAs/GaSb structures, partially compensated quantum Hall effects arising from the electron-hole hybridization were observed. By changing the thickness of each layer, the energy positions of the conduction band and the valence band can be controlled independently. In InAs/AlSb/GaSb structures, we tried to control the hybridization strength by varying the AlSb barrier thickness. Magnetoresistance measurements, in which the magnetic field was applied perpendicular and parallel to the surface, and cyclotron resonance (CR) measurements show that there is a clear transition from the electron-hole-hybridized system to the electron-hole-independent system. The transition point appeared at around the 2-nm-barrier thickness in all experiments, suggesting a dominant role of the overlap of electron and hole wave functions. According to the absorption peak shapes in the CR measurements, the hybridized system can be further classified as strongly hybridized or weakly hybridized. Only in the weakly hybridized system was the Shubnikov–de Haas–like oscillation due to the short-range scattering by the hole potential observed in the electron CR absorption peak.

DOI: 10.1103/PhysRevB.67.195319 PACS number(s): 73.43.Qt, 73.61.Ey, 76.40.+b

I. INTRODUCTION

In InAs/GaSb heterostructures with an appropriate layer thickness, the conduction band in the InAs and the valence band in the GaSb overlap. When the Fermi level lies in the overlap region, electrons in the InAs and holes in the GaSb coexist proximately. This system is of great interest with respect to the electron-hole band hybridization and Coulomb interaction. Hybridization of the conduction band and the valence band makes a minigap at the crossing point due to the interband mixing,[1] so the system is called the hybridized system. The InAs/GaSb system is also expected to exhibit unique physics theoretically, such as an excitonic insulator phase, Bose-Einstein condensation of excitons, and superfluidity of carriers in semiconductors.[2–8] A large number of theoretical and experimental studies have been performed on this system over the past two decades.[9–21] In addition to the physics interests, InAs/GaSb systems are expected to have important device applications such as interband tunnel diodes[9] and midinfrared optical devices.[10,11] A lot of remarkable characteristics, different from those of simple two-dimensional electron or hole systems, have been observed. Regarding the magnetotransport properties observed so far, the most remarkable feature is the partially compensated quantum Hall effect (QHE).[12–15] When the Landau-level filling factors of electrons and holes (ν_e and ν_h) are integers simultaneously, the longitudinal resistance (R_{xx}) becomes zero, and the Hall resistance (R_{xy}) is quantized by the difference in the Landau-level filling factors $R_{xy} = h/e^2|\nu_e - \nu_h|$.[12] However, the principle of the unique QHE has not been clarified yet. Recently, in the case of an almost equal number of electrons and holes, zero-Hall resistance was observed when ν_e and ν_h became the same integers.[13–15] When the magnetic field is applied parallel to the surface, the conduction and the valence band separate from each other in k space and the transition from the hybridized band structure to the truly semimetallic band structure can be observed.[16,17] In addition to the magnetoresistance measurements, cyclotron resonance (CR) measurements have been performed and some characteristics have been discussed in connection with the hybridized band structures.[18–21]

These phenomena should strongly depend on the electron-hole hybridization. It is important to control the hybridization strength to investigate the hybridized system in more detail and realize the new physics phenomena mentioned above. The most suitable way to do this is to insert an AlSb barrier layer between the InAs and the GaSb layers. The AlSb layer acts as a barrier for both the InAs conduction band and the GaSb valence band. However, few about the experimental results on the transport properties in InAs/AlSb/GaSb structures have been reported.[21,22] One of the reasons seems to be difficulty in treating an aluminum source in a metal-organic vapor-phase-epitaxy (MOVPE) system, although MOVPE system enables us to supply high-quality InAs/GaSb heterostructures.

In most previous experimental reports on hybridized system, an InAs layer is sandwiched by GaSb layers.[12–15] Such symmetric structures have some advantages in that the symmetric potential profile makes the band calculation simpler and the electron density can be reduced to the point where it

is almost equal to the hole density. However, symmetric structures also have some disadvantages. There remains the possibility that two GaSb layers with unequal hole densities make the properties complicated. In terms of the crystal growth mechanism, growing an InAs layer on a GaSb layer and growing a GaSb layer on an InAs layer are quite different. Moreover, interface effect caused by the insertion of thin AlSb layers on both sides of the InAs layer makes the properties more complicated. In addition, considering device applications, a *p*-*n*-*p* structure is not suitable for the devices with a *p*-*n* junction. In contrast, for asymmetric structures, such as InAs/GaSb structures sandwiched by AlGaSb layers, holes are definitely confined in one GaSb layer. By varying the thickness of each layer, the electron and hole confinement energies can be controlled independently. The freedom of the band design is expanded, including the modulation doping to the AlGaSb layers. In addition, the structures are applicable to *p*-*n*, and optical devices.

We adopted asymmetric InAs/(AlSb)/GaSb structures grown by molecular beam epitaxy (MBE) to investigate the dependence of the transport properties on the electron-hole coupling strength.[20] In first half of this paper, we present the transport properties in asymmetric InAs/GaSb structures in which each layer has different thickness. In the latter part, we present variations on the transport properties in asymmetric InAs/AlSb/GaSb structures with a different AlSb thickness. The magnetoresistance measurements with the magnetic field applied parallel and perpendicular to the surface and the cyclotron resonance (CR) measurements were performed. We discuss the critical point of the transition from the hybridized system to the electron-hole-independent system. According to the absorption peak shapes in the CR measurements, the hybridized system can be further classified as strongly hybridized or weakly hybridized. Only in the weakly hybridized system was the Shubnikov–de Haas–(SdH–) like oscillation observed in the electron CR absorption peak. We also discuss the origin of the oscillation.

II. SAMPLES AND EXPERIMENTAL PROCEDURES

InAs/(AlSb)/GaSb structures with various electron-hole coupling were grown by MBE. In the MBE method, AlSb can be grown to one-atomic-layer accuracy. The main structures, InAs/(AlSb)/GaSb, are sandwiched between AlGaSb barriers.

A schematic of the sample structure is shown in Fig. 1. First, a GaAs buffer layer was grown on a semi-insulating GaAs substrate. Next, a 200-nm AlSb layer, 10 periods of 25-nm GaSb/ 25-nm AlSb superlattice, a 500-nm $Al_{0.7}Ga_{0.3}Sb$ layer, 10 periods of 25 nm-GaSb/ 25 nm-AlSb superlattice, and a 50 nm-$Al_{0.7}Ga_{0.3}Sb$ layer were grown. Then, a GaSb layer, an AlSb barrier layer (in the case of the InAs/AlSb/GaSb structures) and an InAs layer were grown successively. Finally, a 25-nm $Al_{0.7}Ga_{0.3}Sb$ layer and a 5-nm GaSb cap layer were grown. All layers were nominally undoped. The interface on the both sides of the InAs layer was controlled so that it would be InSb-like.[23]

The schematic energy band diagram of InAs/(AlSb)/GaSb heterostructures is shown in Fig. 2. For InAs/GaSb structures, two series of samples were made. In one, samples have 18-nm wide InAs with GaSb ranging from 12- to 24-nm. In the other, they have 18-nm GaSb with InAs ranging from 12- to 30-nm wide. For InAs/AlSb/GaSb structures, the AlSb barrier thickness was varied from 0.3 to 3.6 nm for the 18-nm InAs layer and the 18-nm GaSb layer. When the confinement energy is ignored, the overlap of the InAs conduction band and the GaSb valence band is 0.15 eV. And the size quantization in the InAs and the GaSb quantum wells reduces the band overlap. In principle, due to the electron transfer from the GaSb to InAs, the electron density in the InAs should be equal to the hole density in the GaSb. In that case, the Fermi level lies in the minigap and the system becomes an insulator. However, in reality, due to the surface potential and the interface defects in the structure, the Fermi level is raised. As a result, the electron density in the InAs is much higher than the hole density in the GaSb.

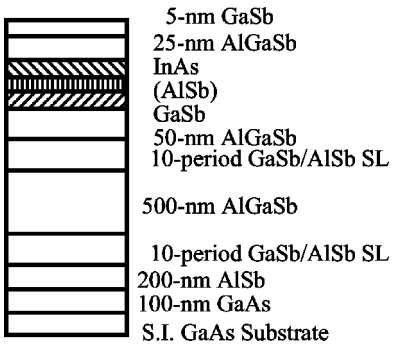

FIG. 1. A schematic of the sample structure. The InAs/(AlSb)/GaSb structure is sandwiched by $Al_{0.7}Ga_{0.3}Sb$ barriers. All layers are undoped. The interfaces on the both sides of the InAs layer are InSb like.

The transport properties were measured in a cryostat at 1.6 K with a superconducting magnet of up to 15 T. Hall bar structures with a width of 50 μm and a voltage probe interval of 180 μm were used for the transport measurement. For the magnetoresistance measurement and the two terminal resistance measurement. The current was 1-μA dc. No significant changes were observed between the dc measurements and the ac lock-in measurements. For the CR measurements,

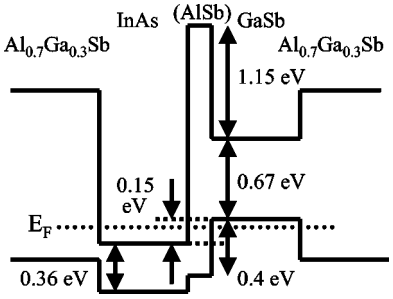

FIG. 2. A schematic energy band diagram of the samples. The overlap of the conduction band in the InAs and the valence band in the GaSb is 0.15 eV. Due to the surface and the interface effects, electrons confined in the InAs layer have larger density than holes in the GaSb layer. The correlation strength between the electrons and holes is controlled by the thickness of the AlSb barrier.

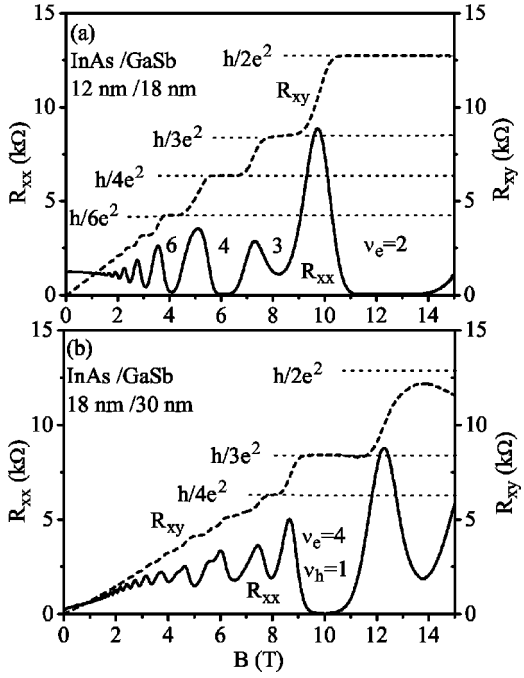

FIG. 3. Typical results of the magnetoresistance measurement in InAs/GaSb samples when the magnetic field was applied perpendicular to the surface. By changing each layer thickness, the system can change from the single-carrier system and the hybridized system. QHE's show clear characteristics of the single-carrier (electron) system (a) (InAs:12nm/GaSb:18 nm), where R_{xy} is quantized by ν_e, and the hybridized system (b) (InAs:18 nm/GaSb:30 nm), where R_{xy} is quantized by $|\nu_e - \nu_h|$.

absorption spectra of far-infrared (FIR) laser emissions from methanol in a cavity pumped by a CO_2 laser were measured as a function of the magnetic field. A Putley-type InSb FIR detector was used.

III. RESULTS AND DISCUSSION

A. InAs/GaSb heterostructures

First, we discuss the experimental results obtained for InAs/GaSb heterostructures. The overlap between conduction and valence bands was modified by the quantum-well thickness through the size quantization effect. Figure 3 shows typical magnetoresistance characteristics measured for InAs/GaSb samples. The magnetic field was applied perpendicular to the surface. For the sample with 12-nm InAs and 18-nm GaSb layers, the QHE clearly shows the characteristics of the single carrier (electron) system [Fig. 3(a)]. The plateaus in R_{xy} are quantized by $h/e^2\nu_e$, and R_{xx} becomes zero in the high magnetic field region when $\nu_e(=nh/eB)$ is an integer, where n is the electron density. The estimated n and the electron mobility (μ_e) are 5.9×10^{15} m^{-2} and 3.0 m^2 V^{-1} s^{-1}, respectively. For a sample with 18-nm InAs and 30-nm GaSb layers, the QHE shows the characteristics of the hybridized system [Fig. 3(b)]. The electron mobility is much larger than the hole mobility and the electron density is larger than the hole density. Therefore, R_{xx} is mainly governed by the electrons. The Shubnikov–de Haas (SdH) oscillation in R_{xx} gives $n=11.4\times10^{15}$ m^{-2}. At 10 T, where $\nu_e=4$, R_{xx} becomes zero, but the plateau in R_{xy} is quantized by the total filling factor $\nu=3$. Therefore, $\nu_h=1$ is expected at the field.[12] Using the above electron density, accurately estimated from the SdH oscillation, and the hole density roughly estimated from the quantized Hall plateau, the classical fitting in the low magnetic field was performed to estimate the electron and hole mobilities, and obtain a more accurate hole density.[24] For this sample, the results are $n=11.4\times10^{15}$ m^{-2}, $\mu_e=4.6$ m^2 V^{-1} s^{-1}, $p=3.8\times10^{15}$ m^{-2}, $\mu_h=0.4$ m^2 V^{-1} s^{-1}, where p is the hole density and μ_h is the hole mobility.

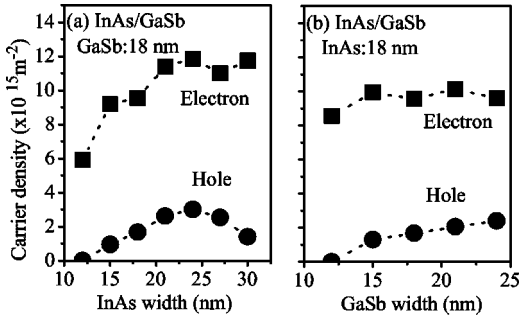

FIG. 4. Electron and hole densities as a function of InAs or GaSb layer thickness. (a) GaSb thickness is fixed at 18 nm. (b) InAs thickness is fixed at 18 nm. When the InAs layer or the GaSb layer thickness is decreased, the system becomes the single-carrier system, due to the enhancement of the confinement energy.

In the above estimation, the premise is existence of holes and electrons. The outer circlelike orbit on the Fermi surface, mainly coming from the InAs conduction band, is regarded as an electron orbit and the inner warped orbit, mainly coming from the GaSb valence band, is regarded as a hole orbit [at the crossing point on the Fermi level in Fig. 6(a)]. When the Fermi level lies much higher than the minigap (our case), carriers behave as those in the original conduction and valence bands. If we consider the hybridization effect, the effect should be included in the mobilities estimated from the classical fitting. If the Fermi level approached to the minigap, a strong hybridization effect on the densities and mobilities would be expected.

Figure 4 shows electron and hole densities obtained for InAs/GaSb systems when the GaSb layer thickness was fixed to 18 nm and the InAs layer thickness was changed (a) and vice versa (b). The Fermi level was assumed to be pinned at a certain potential by the interface states at the InAs/AlGaSb interface. As the InAs thickness increases, the confinement energy of electrons decreases. Therefore, the conduction band bottom becomes much lower and the electron density increases. In the macroscopic view, the total charge should be neutral. As the electron density increases, the hole density should also increase due to the Coulomb attraction. However, the change of the charge balance at the InAs/GaSb interface, which contains defects and other problems, prevents holes increasing. As a result, the gain of the holes is less than that of the electrons. The hole density decreases in the samples having InAs more than 24-nm wide. Although the reason for this is not clear, a complex carrier balance,

TABLE I. Electron and hole densities and mobilities of InAs/AlSb/GaSb samples. The thickness of the InAs layer and the GaSb layer is 18 nm. The AlSb layer thickness is changed.

Sample	AlSb thickness (nm)	$n(\times 10^{15}\ \mathrm{m}^{-2})$	$\mu_e(\mathrm{m}^2\ \mathrm{V}^{-1}\ \mathrm{s}^{-1})$	$p(\times 10^{15}\ \mathrm{m}^{-2})$	$\mu_h(\mathrm{m}^2\ \mathrm{V}^{-1}\ \mathrm{s}^{-1})$
A0	0	9.5	1.1	1.6	0.4
A1	0.3	12.5	1.1	5.0	0.5
A2	0.6	13.7	3.1	5.8	0.4
A3	1.0	14.6	4.0	6.1	0.5
A4	1.8	14.9	13.3	5.6	1.1
A5	3.6	14.5	12.0	6.8	1.1

including band bending, might be induced. In the case of Fig. 4(b), the Fermi level is also pinned at the InAs/AlGaSb interface. As the GaSb layer thickness increases, the confinement becomes smaller. Therefore, the hole density increases. The carrier balance change at the InAs/GaSb interface cancels this hole density increase out so that the electron density is kept almost constant. In both series, the holes are quenched when the InAs or the GaSb layer becomes thinner. Halvorsen *et al.* calculated the energies of AlSb/InAs/GaSb/AlSb structures.[10] However, a precise comparison between experiments and calculation is difficult because of the difference in layer parameters and, moreover, because the important role of interface states is usually neglected in the calculation. Here, we roughly compare experimental results with the calculated energies in AlSb/InAs/AlSb and in AlSb/GaSb/AlSb quantum wells.[10] A comparison between the conduction band bottom of the AlSb/InAs (12 nm)/AlSb quantum well ($E1$) and the valence band top of the AlSb/GaSb (18 nm)/AlSb quantum well ($H1$) reveals that $E1$ lies higher than $H1$. This indicates, the coexistence of electrons and holes is broken. However, when we compare the AlSb/InAs (18 nm)/AlSb quantum well and the AlSb/GaSb (12 nm)/AlSb quantum well, we find $E1$ lies under $H1$. Considering the electron accumulation in the InAs, it is expected that the Fermi-level goes above $H1$. The transition between the hybridized system and the two-dimensional electron system in our results almost agrees with the simple theoretical calculation.

B. InAs/AlSb/GaSb heterostructures

To measure the effect of the AlSb barrier insertion, we selected InAs (18 nm)/GaSb (18 nm) as the starting sample and varied the AlSb barrier layer. The electron and hole densities and mobilities of InAs/AlSb/GaSb samples, estimated from the magnetoresistance characteristics in a high field and the classical fits in a low field, are shown in Table I. Figures 5(a)–5(c) show the typical results of the magnetoresistance measurements for the samples with 0-, 1.8-, and 3.6-nm AlSb barrier layers, respectively. The characteristics of the hybridized system are conserved, when the AlSb barrier is up to 1.8 nm. When both electron and hole Landau-level filling factors are close to integers, the great minima in R_{xx} and the plateaulike structures in R_{xy} quantized by the integer $|\nu_e-\nu_h|$ were observed. For example, in Fig. 5(a), there is a great minimum in R_{xx} and R_{xy} situates around $h/3e^2$ at 9.8 T, where $\nu_e=4$ and $\nu_h=1$. In Fig. 5(b), at 10.2 T, R_{xx} has a minimum and R_{xy} is situated at $h/3e^2$, where $\nu_e=6$ and $\nu_h=3$. However, for the sample with a 3.6 nm barrier, a two-dimensional electron systemlike periodic oscillation and a large oscillation in R_{xy} synchronized by the R_{xx} oscillation were observed. When the thick AlSb barrier is inserted, the electrons and the holes are separated from each other and

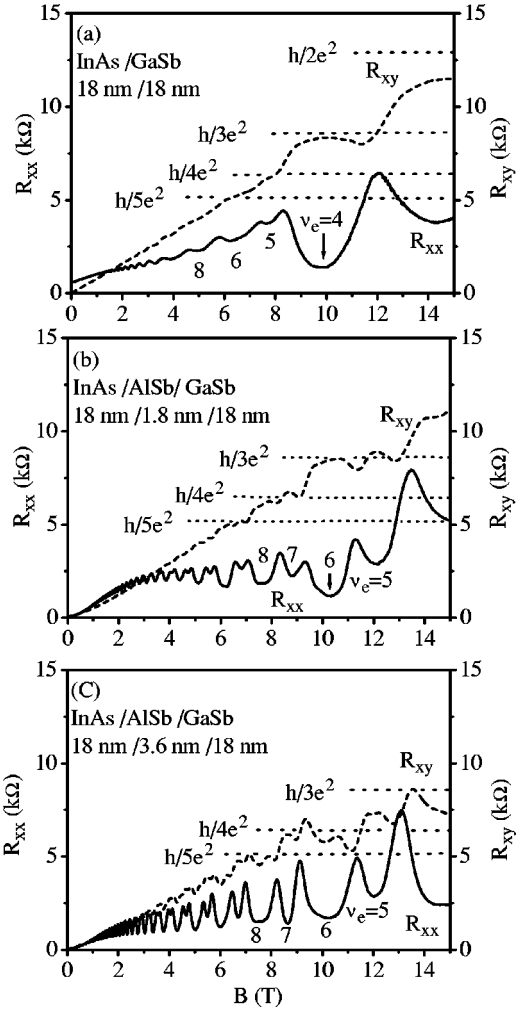

FIG. 5. Typical results of the magnetoresistance measurements in InAs/AlSb/GaSb heterostructures. (a) Without an AlSb barrier, (b) 1.8-nm AlSb barrier, (c) 3.6-nm AlSb barrier. For a barrier of up to a 1.8 nm, the hybridized system is conserved, i.e.; great minima were observed in R_{xx} (arrowed) and R_{xy} is almost totally quantized by $|\nu_e-\nu_h|$ when both ν_e and ν_h become integers.

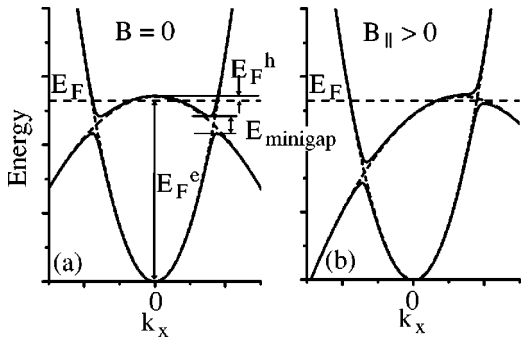

FIG. 6. Schematic diagram of electron and hole dispersion relations in hybridized band structures without a magnetic field (a) and with a magnetic field parallel to the surface (b). In the hybridized system, minigaps appear at the crossing points of the conduction band and the valence band. When the parallel magnetic field is applied, the conduction band and the valence band separate. When the minigap goes through the Fermi-level, a resistance maximum is expected.

behave independently. It is expected that the system is no longer the hybridized system, but the electron-hole-independent system instead. When the electron and the hole QHEs occur simultaneously and independently, the difference of the Hall voltages causes current to flow along the transverse direction. Therefore, R_{xx} diverges from zero resistance due to the Hall conductance matrix element (σ_{xy}), and R_{xy} is affected repeatedly.

In addition to the magnetoresistance measurements in which the magnetic field was applied perpendicular to the surface, we measured the two-terminal resistance, applying the magnetic field parallel to the surface. Using this measurement, the existence of the minigaps was confirmed. Figure 6 shows schematic diagrams of the dispersion relations without a magnetic field (a) and with a parallel magnetic field (b). When the barrier is thin enough, the conduction band and the valence band are hybridized and the minigaps appear at the crossing points. Without a magnetic field, the Fermi level lies above the minigaps because there are many more electrons than holes [Fig. 6(a)]. Applying the magnetic field ($B_\parallel$) in the [010] direction, the conduction band and the valence band separate. The relative separation between them ($\delta\mathbf{k}$) is given by

$$\delta k_x = \frac{eB_\parallel \langle z \rangle}{\hbar}, \tag{1}$$

where $\langle z \rangle$ is the distance between the average positions of the electrons and the holes in real space. At a certain magnetic field, a part of the minigaps goes through the Fermi-level, and a resistance maximum is expected [Fig. 6(b)].[17,25] We simulated the minigap size dependence of the resistance changes as a function of the magnetic field using the same method used by Lakrimi *et al.*[17] The upper inset in Fig. 7 shows the typical simulated resistance with $\Delta = 17$ meV, and Fig. 7 shows the peak positions of the resistance maxima in the magnetic field as a function of Δ deduced from the simulation, where Δ is the coupling energy related to the minigap size and is the energy separation at the crossing point of the

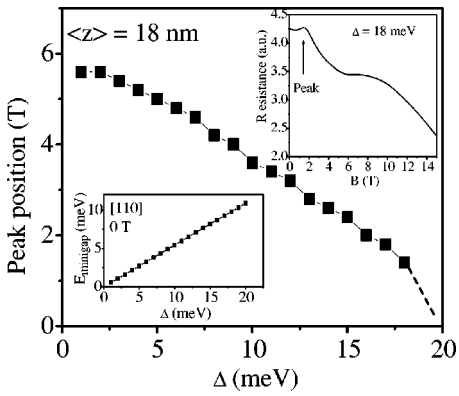

FIG. 7. Simulated resistance maximum peak positions in the magnetic field as a function of the coupling energy Δ related to the minigap size. The upper inset shows the typical simulated resistance changes with $\Delta = 18$ meV. A magnetic field applied in the [010] direction is assumed. The lower inset shows the discrepancy between Δ (the energy difference at the crossing point of the bands in k space) and the real minigap size (the energy difference between the minimum in the upper band and the maximum in the lower band in the [110] direction). When the original conduction band is steep and the valence band is gradual, the discrepancy becomes large.

original conduction and the valence bands in k space.[17] For the valence band, dispersion parameters of bulk material were used. Other parameters were estimated as for the no-barrier sample, where the electron effective mass $m_e = 0.048 m_0$, as evaluated by the CR measurement (discussed later), the Fermi energy from the conduction band bottom $E_F^e = 47.4$ meV, and the Fermi-energy from the valence band top $E_F^h = 2.1$ meV. The $\langle z \rangle$ was set to 18 nm, which is the distance between centers of the InAs layer and the GaSb layer. The temperature was set to 4.2 K considering an adequate broadening. In the case of small Δ, the peak positions are identified as the crossing points of the original conduction and valance bands. With increasing Δ, the peak shifts lower in the magnetic field. In the case of large Δ, the resistance has a maximum at 0T and the peak changes to a shoulder near 0 T.

Taking the results of the simulation into consideration, we discuss the experimental results. Figure 8 shows the experimental results for each sample. The magnetic field is applied to the [010] direction. For samples having thin barriers up to 1.8 nm the resistance has a maximum at a certain magnetic field (arrows in Fig. 8). This shows the existence of the minigaps. The thinner the barrier becomes, the lower in the magnetic field the position of the maximum shifts. This is easily understood as the minigaps becoming larger with decreasing barrier thickness. By comparing the simulation with the experimental result for the no-barrier sample, Δ is estimated to be 18 meV. When the original conduction band is steep and the valence band is gradual, the discrepancy of Δ from the minigap size becomes large (see the lower inset of Fig. 7). Considering this effect, the real minigap is expected to be about half of Δ. However, this value is still too large compared with the reported value.[1,17] Although the reason is not completely clear, this discrepancy can be explained to some extent by taking into account the larger distance between

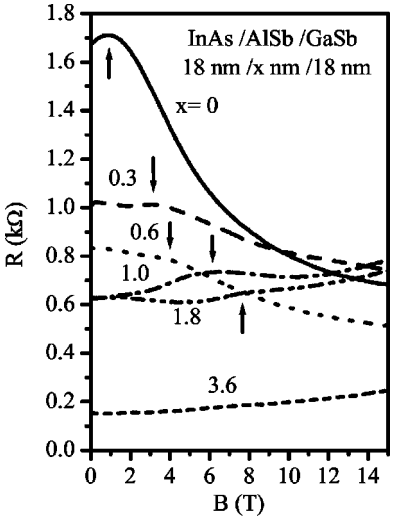

FIG. 8. Two-terminal resistances in InAs/AlSb/GaSb heterostructures. When the magnetic field is applied parallel to the surface, the [010] direction. For up to a 1.8-nm barrier, the resistance maxima were observed (arrows), suggesting the existence of the minigap. For the 3.6-nm barrier sample, the resistance is little changed. The measured two-terminal resistances is affected by the contact resistance of the Ohmic contacts and deviates from the resistance value estimated from the carrier densities and mobilities at $B=0$.

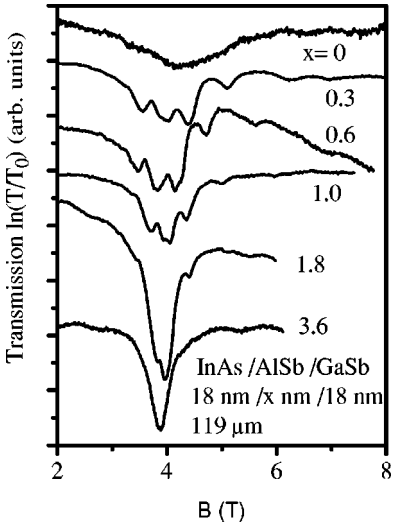

FIG. 9. FIR absorption spectra in InAs/AlSb/GaSb heterostructures. Absorption peaks around 3.9 T is due to electron CR. Up to a 1.8-nm barrier (excluding the no-barrier sample), oscillating behavior in the CR peak due to the short-range scattering was observed. For the 3.6-nm-barrier sample, a sharp CR peak without oscillation was observed.

electrons and holes.[26] Compared with other samples, the no-barrier sample has many more electrons than holes. This means that the charge transfer from the GaSb layer to the InAs layer is small and electrons are mainly provided from the neighboring AlGaSb barrier and the InAs/AlGaSb interface defects. As a result, ionized donors at the interface attract electrons separating from holes. Therefore, $\langle z \rangle$ in the experiment should be larger than 18 nm and the corresponding minigap should be smaller. Furthermore, the large anisotropy of the valence band may affect the discrepancy, because E_F^h is compatible with minigaps.

Assuming the minigap size for the 1.8-nm barrier sample close to zero and the first crossing at 7.7 T with the parameters for the 1.8-nm sample of $E_F^e=81.1$ meV, $E_F^h=7.2$ meV, and $m_e=0.044\ m_0$, we obtain $\langle z \rangle = 16$ nm. This must be because the electrons and the holes are close to each other due to the Coulomb attraction. These experimental results show that the $\langle z \rangle$ value changes from 16 to 30 nm depending on the charge balance between electrons, holes, and interface charges. The effect of the AlSb barrier thickness is less important because the barrier thickness is much smaller than the thickness of the InAs and GaSb layers.

In contrast with the thin-barrier samples, the sample with a 3.6-nm barrier shows little resistance change. The resistance simply increases as a function of the magnetic field, though the electron and the hole densities are almost the same as those of the sample with a 1.8-nm barrier. This means there is no band hybridization and that the conduction band in the InAs and the valence band in the GaSb exist independently. It is noteworthy that the band hybridization disappears at AlSb barrier thickness between 1.8 and 3.6 nm, which is the thickness range where the partially compensated quantum-Hall effect also disappears (Fig. 5).

The transition between the hybridized system and the independent system also appears in the CR measurements. Figure 9 shows the FIR absorption spectra as a function of the magnetic field. The radiated laser wavelength was 119 μm. Absorption peaks around 3.9 T are due to the electron cyclotron resonance. The effective mass (m_{CR}^*) estimated from the results is 0.043 m_0 (3.6-nm AlSb) $\sim$0.048 m_0 (no barrier). The value for InAs bulk ($m_{\rm bulk}^*$) is 0.023 m_0. The large conduction band nonparabolicity due to the confinement makes the effective mass much larger. We roughly estimate energy dependence of the effective mass [$m^*(E)$], assuming an infinite InAs quantum well, as

$$m^*(E)=m_{\rm bulk}^*\left(1+\frac{2E}{E_g}\right),$$

where $E=E_0+E_F^e$, $E_0(=\hbar^2\pi^2/2m_{\rm bulk}^*L^2)$ is the confinement energy of the lowest subband and L (=18 nm) is the InAs layer thickness.[27] The InAs band gap energy E_g =360 meV is used. Then,

$$m^*(E)=0.035\ \ m_0\ \ \text{(no barrier)}$$
$$\sim 0.040\ \ m_0\ \ \text{(3.6-nm AlSb)}$$

is obtained, the value of which depends on the electron density estimated in Table I. The measured effective masses are larger than the calculated ones. A lot of factors make the effective mass larger: an effective electron layer thickness smaller than L due to the band bending, band hybridization, strain for the lattice mismatch, and penetration of the electron wave function to the barriers.[18,19,21,28,29] In our experiments, the effective mass became larger with decreasing

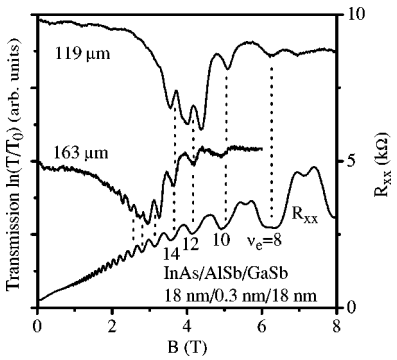

FIG. 10. FIR absorption spectra of the 0.3-nm-AlSb barrier sample radiating different FIR lines. R_{xx} is also plotted. The oscillation period in the CR absorption peaks is consistent with the integer ν_es in the SdH oscillation and the oscillation turns over at the peak center.

AlSb barrier thickness, suggesting the important role of the band hybridization effect on the enhanced nonparabolicity of the conduction band.

For thin-barrier samples of up to 1.8 nm (excluding the no-barrier sample), oscillating behavior was observed in the CR absorption peak. In these samples, the electron and hole bands are weakly hybridized, so we classified them as weakly hybridized. The oscillation does not appear for the 3.6-nm-barrier sample . To investigate the origin of the oscillation in the CR absorption peak, FIR absorption spectra with a different wavelength were measured. Figure 10 shows the FIR absorption spectra for the 0.3-nm-barrier sample with 163- and 119-μm radiations. R_{xx} without radiation is also plotted. The oscillation on the CR absorption peak is consistent with the SdH oscillation in R_{xx} and turns over at the center of the absorption peak. This phenomenon is known as short-range scattering and observed in Si-inversion structures.[30,31] Vasilyev *et al.* observed similar oscillation in GaSb/InAs/GaSb quantum wells.[22] They concluded that the scattering is caused by the potential coming from the interface roughness, although they mentioned the possibility that it is caused by the screened hole potential. In our case, however, the oscillation was observed for samples with up to a 1.8-nm barrier and not observed for that with the 3.6-nm barrier. The conditions of the interfaces are almost the same for the 1.8-nm- and 3.6-nm-barrier samples. Therefore, we can neglect interface roughness as the origin of the oscillatory behavior. The most plausible explanation is electron scattering by hole potential. The Fermi wavelength of an electron with $n \simeq 14 \times 10^{15}$ m^{-2} is 21 nm and the averaged hole separation with $p \simeq 5 \times 10^{15}$ m^{-2} is 14 nm. The matching between electron wavelength and hole separation induces strong electron scattering due to a potential fluctuation originating from holes. This scattering may be enhanced when the electron wave is pushed to the hole potential, i.e., the overlap between electron and hole wavefunctions is large. As mentioned earlier, the results of the magnetoresistance measurements when the magnetic field was applied parallel or perpendicular to the surface show little electron-hole coupling for the 3.6-nm-barrier sample, suggesting small scattering by the hole potential. There was also no oscillation in the CR absorption peak for the no-barrier sample, classified as the strongly hybridized system. Although the reason is not clear, there are several possibilities. In the no-barrier sample, the coupling between electrons and holes is very strong and there appears a large minigap. Such band hybridization may make the oscillation broader. Carriers in the system may not be treatable under the concept of electrons and holes any longer. In addition, removal of the AlSb barrier makes a large difference in the interface characteristics. Both electron and hole densities decrease and the mobilities also decrease. The SdH oscillation is not well resolved for the no-barrier sample [in Fig. 5(a)]. Therefore, it is also expected that the imperfect Landau-level splitting makes the oscillation less clear.

IV. CONCLUSIONS

We made asymmetric InAs/GaSb and InAs/AlSb/GaSb heterostructures sandwiched by AlGaSb layers grown by MBE and measured the magnetoresistance and CR absorption. For the InAs/GaSb heterostructures, a clear partially compensated QHE that is the same as that reported for GaSb/InAs/GaSb quantum wells was observed. By varying each layer thickness, the energy positions of the conduction band and the valence band can be controlled independently. The transport characteristics change from those of the hybridized system to those of the two-dimensional electron system. For the InAs/AlSb/GaSb heterostructures, the strength of the hybridization is controlled by the AlSb barrier thickness. The system is classified as strongly hybridized, weakly hybridized, or a electron-hole-independent systems. In the independent system for samples with an AlSb barrier more than 2-nm thick, all experimental results show the carriers move independently without the hybridization effect. The magnetoresistance measurement with the magnetic field parallel to the surface shows no minigap. In the CR measurement, a sharp absorption peak coming from the electron CR was observed. In the strongly hybridized system for the sample without an AlSb barrier, the transport properties show the characteristics of the hybridized system. A partially compensated QHE was observed, and a large maximum in the magnetoresistance with the magnetic field parallel to the surface was observed. A broad absorption peak due to the electron cyclotron resonance was observed. In the weakly hybridized system for samples with a thin AlSb barrier, the characteristics of the hybridized system shown in the magnetoresistance measurements are conserved. In the CR measurements, the Shubnikov–de Haas–like oscillation due to the short-range-scattering by the hole potential was observed in the electron CR absorption peak.

ACKNOWLEDGMENTS

We thank Dr. Takaaki Mukai for his encouragement throughout this work. This work was partly supported by the NEDO International Joint Research Programs ''NTDP-98'' and ''Nano-elasticity.''

[1] M. Altarelli, Phys. Rev. B **28**, 842 (1983).
[2] D. Jérome, T. M. Rice, and W. Kohn, Phys. Rev. **158**, 462 (1967).
[3] E. G. Wang, Y. Zhou, C. S. Ting, J. Zhang, T. Pang, and C. Chen, J. Appl. Phys. **78**, 7099 (1995).
[4] S. de-Leon and B. Laikhtman, Phys. Rev. B **61**, 2874 (2000).
[5] V. A. Fedorin, Fiz. Tverd. Tela (S.-Peterburg) **24**, 279 (1982).
[6] Y. Naveh and B. Laikhtman, Phys. Rev. Lett. **77**, 900 (1996).
[7] S. Datta, M. R. Melloch, and R. L. Gunshor, Phys. Rev. B **32**, 2607 (1985).
[8] X. Xia, X. M. Chen, and J. J. Quinn, Phys. Rev. B **46**, 7212 (1992).
[9] H. Kitabayashi, T. Waho, and M. Yamamoto, Appl. Phys. Lett. **71**, 512 (1997).
[10] E. Halvorsen, Y. Galperin, and K. A. Chao, Phys. Rev. B **61**, 16 743 (2000).
[11] H. Ohno, L. Esaki, and E. E. Mendez, Appl. Phys. Lett. **60**, 3153 (1992).
[12] E. E. Mendez, L. Esaki, and L. L. Chang, Phys. Rev. Lett. **55**, 2216 (1985).
[13] K. S. H. Dalton, M. van der Burgt, M. Lakrimi, R. J. Warburton, M. S. Daly, W. Lubczyński, R. W. Martin, D. M. Symons, D. J. Barnes, N. Miura, R. J. Nicholas, N. J. Mason, and P. J. Walker, Surf. Sci. **305**, 156 (1994).
[14] M. S. Daly, K. S. H. Dalton, M. Lakrimi, N. J. Mason, R. J. Nicholas, M. van der Burgt, P. J. Walker, D. K. Maude, and J. C. Portal, Phys. Rev. B **53**, R10 524 (1996).
[15] R. J. Nicholas, K. Takashina, M. Lakrimi, B. Kardynal, S. Khym, N. J. Mason, D. M. Symons, D. K. Maude, and J. C. Portal, Phys. Rev. Lett. **85**, 2364 (2000).
[16] M. J. Yang, C. H. Yang, B. R. Bennett, and B. V. Shanabrook, Phys. Rev. Lett. **78**, 4613 (1997).
[17] M. Lakrimi, S. Khym, R. J. Nicholas, D. M. Symons, F. M. Peeters, N. J. Mason, and P. J. Walker, Phys. Rev. Lett. **79**, 3034 (1997).
[18] J. Kono, B. D. McCombe, J.-P. Cheng, I. Lo, W. C. Mitchel, and C. E. Stutz, Phys. Rev. B **55**, 1617 (1997).
[19] T. P. Marlow, L. J. Cooper, D. D. Arnone, N. K. Patel, D. M. Whittaker, E. H. Linfield, D. A. Ritchie, and M. Pepper, Phys. Rev. Lett. **82**, 2362 (1999).
[20] J. H. Roslund, K. Saito, K. Suzuki, H. Yamaguchi, and Y. Hirayama, Jpn. J. Appl. Phys., Part 1 **39**, 2448 (2000).
[21] Yu. Vasilyev, S. Suchalkin, K. von Klitzing, B. Meltser, S. Ivanov, and P. Kop'ev, Phys. Rev. B **60**, 10 636 (1999).
[22] Yu. B. Vasilyev, S. D. Suchalkin, S. V. Ivanov, B. Ya. Mel'tser, A. F. Tsatsul'nikov, P. V. Neklyudov, and S. Kop'ev, Fiz. Tekh. Poluprovodn. (S.-Peterburg) **31**, 1246 (1997).
[23] G. Tuttle, H. Kromer, and J. H. English, J. Appl. Phys. **67**, 3032 (1990).
[24] R. A. Smith, *Semiconductors* (Cambridge University Press, Cambridge, 1978), p. 114.
[25] J. A. Simmons, S. K. Lyo, N. E. Harff, and J. F. Klem, Phys. Rev. Lett. **73**, 2256 (1994).
[26] When we assume $\langle z \rangle = 30$ nm, the peak positions of 1.2 T can be reasonably explained by $\Delta = 16$ meV, corresponding minigap of 8 meV.
[27] J. Scriba, A. Wixforth, J. P. Kotthaus, C. R. Bolognesi, C. Nguyen, G. Tuttle, J. H. English, and H. Kroemer, Semicond. Sci. Technol. **8**, S133 (1993).
[28] P. J. Lin-Chung and M. J. Yang, Phys. Rev. B **48**, 5338 (1993).
[29] M. J. Yang, P. J. Lin-Chung, B. V. Shanabrook, J. R. Waterman, R. J. Wagner, and W. J. Moore, Phys. Rev. B **47**, 1691 (1993).
[30] T. Ando, J. Phys. Soc. Jpn. **38**, 989 (1975).
[31] G. Abstreiter, J. P. Kotthaus, and J. F. Koch, Phys. Rev. B **14**, 2480 (1976).